Applied Catalysis A: General 423–424 (2012) 7–14

Contents lists available at SciVerse ScienceDirect

Applied Catalysis A: General

journal homepage: www.elsevier.com/locate/apcata

Influence of ethanol in the presence of H_2 on the catalytic growth of vertically aligned carbon nanotubes

O. Guellati[a,b], I. Janowska[a,*], D. Bégin[a], M. Guerioune[b], Z. Mekhalif[c], J. Delhalle[c], S. Moldovan[d], O. Ersen[d], C. Pham-Huu[a]

[a] Laboratoire des Matériaux, Surfaces et Procédés pour la Catalyse (LMSPC), ECPM - UMR 7515 CNRS, Université de Strasbourg, 25 rue Becquerel, 67087 Strasbourg Cedex 02, France
[b] Laboratoire d'Etude et de Recherche des Etats Condensés (LEREC), Dép. de Physique, Université Badji Mokhtar BP, 12, Annaba 23000. Centre Universitaire de Souk-Ahras, BP. 1553, Souk-Ahras 41000 Algeria
[c] Laboratoire de Chimie et d'Électrochimie des Surfaces (CES), FUNDP rue de Bruxelles 61, B-5000 Namur, Belgium
[d] Institut de Physique et Chimie des Matériaux de Strasbourg (IPCMS), UMR 7504 du CNRS, Université de Strasbourg France

ARTICLE INFO

Article history:
Received 28 October 2011
Received in revised form 25 January 2012
Accepted 10 February 2012
Available online 27 February 2012

Keywords:
VA-MWNTs
Floated-catalyst
Ethanol-CCVD

ABSTRACT

The vertically aligned multi-walled carbon nanotubes (VA-MWNTs) were synthesized by a catalytic chemical vapor deposition (CCVD) technique, using ferrocene as an iron catalyst precursor and toluene/ethanol mixture with different ratio as a carbon source/etching agent, in the presence of H_2. The growth rate, efficiency and the structure of the synthesized tubes were investigated. The CNTs growth rate and quality of tubes significantly improve up to 9 vol.% of ethanol whereas a negative influence was observed for higher ethanol concentration (>17 vol.%). Low ethanol content in the reaction mixture (5 vol.%) results in the highest volume density of the tubes within the array along with highest specific surface area. The synergetic effect of EtOH/hydrogen on the growth rate of VA-MWNTs was observed as well.

1. Introduction

Carbon nanotubes (CNTs), a one-dimensional carbon materials with high aspect ratio (the aspect ratio is defined as the length divided by diameter of the nanotube), have received an over increasing scientific interest during the last decades due to their exceptional physical and chemical properties [1–3]. Several advantages such as important mechanical resistance, high electron and thermal conductivity make them interesting for the electronic and reinforcement composite applications. High and fully accessible external surface render them an interesting candidate for catalytic applications. Recent works have pointed out the possible use of carbon nanotubes, either pure or doped with heteroatoms, as catalyst or catalyst support in several reactions [4–7]. The nanoscopic dimension of the CNTs also significantly reduces the problem of diffusion, especially in the case of liquid-phase reaction. Attempts to prepare structured catalytic layers based on vertically aligned CNTs have been reported by several groups working in this field [8,9]. Compared to agglomerated CNTs in powder form, aligned CNTs exhibit several advantageous properties, such as high orientation degree, high purity and easy to be processed regarding the downstream applications [10–13]. Such structured catalyst support allows a development of 3D ordered nanomaterials for several catalytic applications, i.e. support for 3D ordered proton exchange membrane fuel cell (PEMFC) [14,15], catalyst for fine chemical reactions [16,17], selective filter for heavy hydrocarbon separation or virus removal from the water medium [18]. Vertically aligned CNTs can only be synthesized with high rate and purity by CVD methods. It is expected that synthesis environment [19–22], i.e. gas phase composition and flow rate, synthesis temperature and pressure, plays an important role in the morphology and structural change of the active metal catalyst which significantly modify the physical properties and morphology of the final VA-CNTs. Despite the relatively large work devoted to the synthesis of VA-MWNTs by CCVD with immobilized catalyst [23,24], floated CCVD technique [25,26] presents the most promising synthesis method for economically producing large quantities of CNTs in macroscopic form. Additional work is needed in order to improve the CNTs growth rate (yield improvement) and also to reduce as much as possible the amount of amorphous carbon on the surface of the final CNTs (quality improvement). The yield and quality improvement can be achieved when oxidant, i.e. H_2O, O_2, CO_2, CH_3CH_2OH, is added to the feed [27–29]. However, even if this addition method has been comprehensively studied, the influence of alcohol on the overall growth process and quality of the carbon nanotubes has been far

* Corresponding author. Tel.: +33 368852633; fax: +33 368852674.
E-mail address: janowskai@unistra.fr (I. Janowska).

0926-860X/$ – see front matter © 2012 Elsevier B.V. All rights reserved.
doi:10.1016/j.apcata.2012.02.036

much less taken into consideration. Some results concerning the influence of ethanol on the CNTs growth rate have been reported by Terrones and co-workers [30].

Hata et al. [31,32] have reported that the amorphous carbon formed either on the catalyst or on the CNTs walls, can be efficiently removed by adding a small amount (typically <1000 ppm) of steam in the ethylene processing feed. In such synthesis, the oxidant plays a role of an etching agent which allow the removal of carbon species that are not consumed by the CNTs formation and thus, preventing the deactivation of the growth catalyst by amorphous carbon encapsulation. Oxygen [33] and air [34] have also been used to improve the CNTs forest growth by removing the amorphous carbons from the catalyst surface. Ethanol is one of the species containing oxygen, which was also employed directly as carbon source for growing VA-CNTs, instead of hydrocarbons [15,33,35,36]. As mentioned previously [21,28], compare to the CNTs synthesis from liquid hydrocarbons, alcohols provide a better control over the structures of the CNTs. The —OH radical groups and water issued from the decomposition of the ethanol, present in the feed allow the in situ oxidation of the amorphous carbon formed during the synthesis yielding CNTs with better quality. The oxygenated species generated during the growth process also actively participate in the cleaning of the growth catalyst from amorphous carbon preventing their encapsulation and providing higher available growth sites for the CNTs growth. Zhang et al. [37] have showed that ethanol was completely dissociated on the catalyst surface. However, the oxygen-containing species concentration should be limited in order to prevent undesired combustion of the formed CNTs. Furthermore, oxidation at high temperature could also lead to the formation of defects on the carbon nanotube sidewall which significantly decreases the oxidative resistance of the material.

The present study reports on the influence of ethanol concentration, on the intrinsic growth rate and the density of the vertically aligned carbon nanotubes as well as on their graphitization degree through in situ etching of amorphous carbon from the catalyst surface and the tube wall. Although the general conditions of the CVD synthesis are quite similar to the ones reported by Terrones and co-workers [30], i.e. the use of ferrocene/toluene/EtOH mixture, comparable temperature; important differences rise from the much higher concentration of added EtOH (up to 45 vol.% in our case), lower space velocity of the reaction mixture and an addition of H_2. The as-synthesized CNTs are characterized by several techniques and the influence of ethanol concentration during the synthesis of nanotubes on both, the growth rate and the CNTs characteristics is discussed. The characterization results also allow us to determine the optimum concentration of ethanol and the effect of hydrogen in the processing feed in order to obtain vertically aligned CNTs with highest yield and graphitization quality.

2. Experimental

2.1. Vertically aligned carbon nanotubes (VA-MWNTs) array synthesis

The VA-MWNTs synthesis was carried out using floated-catalyst CVD method involving liquid aerosol containing the catalyst precursor (ferrocene, $FeCp_2$ (~2.5 wt.%)) solubilized in toluene and ethanol (carbon sources). The influence of the ethanol concentration on the growth process was investigated using different ethanol-to-toluene concentrations, i.e. 0–45 vol.%. VA-MWNTs were grown on cleaned SiO_2/Si substrate (Siltronix, Si_{100}, 525 μm) covered by a homogeneous SiO_2 layer (100 nm) or directly on a quartz plate. The growth reaction was performed in a cylindrical quartz reactor housed inside an electrical tubular furnace (two independent heating zones). The reactant mixture velocity and growth temperature were maintained at 0.33 mL/min and 870 °C, respectively. The reactant mixture was carried inside the synthesis zone with a stream of H_2 (7 vol.%) in argon with a total flow rate of 1.5 L/min.

The synthesis sequence is following:the reactor was flushed with an argon flow (1.5 L/min STP) during 30 min then the H_2 (100 mL/min STP, ~7 vol.%) was added to the argon flow. The reactor temperature was raised from room-temperature to 870 °C in 1 h. At this temperature, the toluene/ferrocene/ethanol mixture was simultaneously injected with the H_2/Ar flow using a syringe pump during 60 min. After the synthesis, the reactor was cooled down under Ar/H_2 flow. During the synthesis, CNTs are formed on both, the SiO_2/Si plate and on the wall of the quartz reactor. For the more accurate comparison of the influence of the ethanol addition on the overall growth process, only the products from the substrate (SiO_2/Si substrate) were collected and investigated. The thermal decomposition of ethanol generally leads to the formation of water which plays the role of etching agent along with the oxygenated containing species. However, the set-up used did not allow us to monitoring the water evolved during the synthesis.

The synthesized nanotubes arrays were purified from the iron remains by the acid treatment (HCl:HNO_3 = 1:3) at 80 °C for 2 h, washed and dried at r.t. for 24 h then at 100 °C for 2 h.

2.2. Characterization techniques

The morphology of the VA-MWNTs was examined by scanning electron microscopy (SEM) on a JEOL 6700-FEG microscope. The product was fixed on the sample holder by a graphite paste for examination. Before analysis, the sample was covered by a thin layer of gold in order to avoid the problems of charge effect.

High magnification transmission electron microscopy (TEM) was carried out on a JEOL 2100F working under an accelerated voltage of 200 kV with a point-to-point resolution of 0.23 nm. The sample was crushed in a powder form and dispersed by ultrasounds in an ethanol medium for few minutes and a drop of this suspension was deposited onto a holey carbon coated copper TEM grid for examination.

Specific surface area measurements were carried out on a Tristar (Micromeritics) sorptometer using nitrogen as adsorbent at liquid nitrogen temperature. Before measurements, the sample was outgassed at 250 °C for 3 h in order to desorb impurities and moisture from its surface.

Thermal gravimetry analyses (TGA) were carried out in a Q5000 apparatus (TA instrument) under air flow (20 mL/min). The temperature was increased from room temperature to 1000 °C with a heating rate of 10 °C/min.

Raman spectroscopy was carried out on a Microraman RENISHAW spectrometer (RAMASCOPE 2000 with a spot size of 1 μm^2 and 1 cm^{-1} resolution) working with a He–Ne Laser beam with 632.8 nm wavelength. The D/G peak intensity ratio was studied to determine the defective graphitic carbon (1350 cm^{-1}) to graphitic (1589 cm^{-1}) carbon ratio present inside the synthesized CNTs.

XPS analyses were performed with a MULTILAB 2000 (THERMO) spectrometer equipped with Al Kα anode ($h\nu$ = 1486.6 eV) during 10 min of acquisition in order to achieve a good signal-to-noise ratio. Peak deconvolutions were made with the "Avantage" program from Thermo Electron Company. The C1s photoelectron binding energy was set at 284.6 ± 0.2 eV relatively to the Fermi level and used as reference for calibrating the other peak positions.

3. Results and discussion

The representative SEM micrographs of the tubes array synthesized during 1 h in the presence of ferrocene-toluene with 0% of

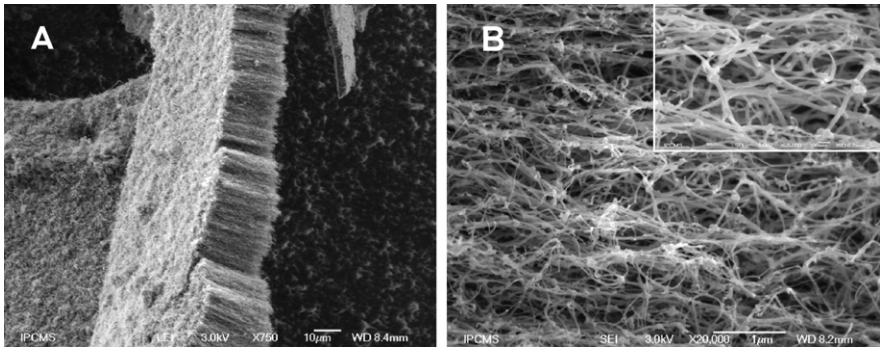

Fig. 1. SEM micrographs of the VA-MWNTs array synthesized in the presence of $FeCp_2$-toluene mixture and H_2 (7 vol.%) at 870 °C for 1 h: (a) low-magnification showing the thickness of the CNTs carpet, (b) high-magnification showing the morphology and alignment of the CNTs within the carpet, inset:micrograph evidencing the high selectivity of the synthesis towards the CNTs formation.

ethanol and 7 vol.% of H_2 are presented in Fig. 1. Low magnification SEM observation indicates that the tubes array is relatively thin with an average height of around 20 μm (Fig. 1A). High magnification SEM observation reveals the relatively high anisotropy of the formed CNTs with an average external diameter centered at around 40 nm (Fig. 1B). SEM analyses also indicate the absence of carbon nanoparticles in the sample which confirm the high selectivity of the synthesis method towards CNTs formation (inset of Fig. 1B). Similar results have already been reported by Janowska et al. [24] using a reactant mixture of ferrocene and toluene without adding hydrogen. However, it is worthy to note that the rate of VA-MWNTs growth and the external diameter of the tubes in Ref. [24] were much higher compared to those obtained in the present work, i.e. 5.0 μm min^{-1} instead of 0.3 μm min^{-1} and 100 nm instead of 40 nm, respectively. These mentioned structural differences result from the difference in terms of the synthesis conditions, i.e. the absence of hydrogen in the reactant mixture and the lower synthesis temperature.

The similar conclusion can be state from the work of Terrones [30] where H_2 was not present in the reaction mixture and where in the case of 0% ethanol the nanotubes carpet was much higher than in this work, 440 μm instead of 20 μm.

High-resolution SEM micrographs (Fig. 1B) also indicate the presence of some lateral growth. Such branching process could be originated from the adsorption of some iron catalyst on the as-grown carbon nanotubes sidewall defects which further initiated secondary growth process leading to the formation of branched nanotubes.

The representative SEM micrographs, with two different magnifications, of the nanotubes arrays synthesized in the presence of various concentrations of ethanol, (5, 9, 17 and 45 vol.%), are presented in Fig. 2. According to the results, the average height of the CNTs carpet is strongly influenced by the concentration of ethanol in the feed keeping other reaction conditions similar. The average height of the CNTs carpet and the corresponding exterior diameter of tubes are plotted as a function of ethanol concentration (Fig. 3A and B). One can state that ethanol concentration up to 9 vol.% has a significant positive influence on the growth rate of the nanotubes carpet. Indeed, the average height of the last steadily increases from 20 μm (0 vol.% ethanol) to about 560 μm (5 vol.% ethanol) and finally to 1100 μm (9 vol.% ethanol); which correspond to the growth rate of 0.3, 9.0 and 18 μm min^{-1}, respectively. High magnification SEM analysis (Fig. 2B and D) also indicates the complete absence of any carbon nanoparticles on the outer surface of the as-synthesized CNTs and confirms the high selectivity of the synthesis method towards the formation of CNTs. It is worthy to note that the average diameter of carbon nanotubes remains almost unchanged as a function of ethanol concentration up to 9 vol.%, according to the high-resolution SEM analysis, which indicates that ethanol, at low concentration, only influences growth rate and hardly influences the carbon nanotubes diameter. According to these results which are not in contradiction with those obtained in Ref. [30], it is evident that an addition of ethanol with low concentration to the reactant mixture, either in the presence of H_2 or not, significantly increases the CNTs growth. It is expected that at low ethanol concentration (<9 vol.%) the oxygenated species generated from the ethanol decomposition could oxidize the residual amorphous carbon on the growth catalyst surface and thus, provide active site for further growth process and consequently leads to an improvement of the CNTs yield. The CNTs formed in the presence of ethanol, i.e. <9 vol.%, also exhibit lower degree of branching according to the SEM analysis (Fig. 2A–D), compared to that observed in the synthesis without ethanol (Fig. 1A and B). Such phenomenon could be explained by the fact that ethanol actively participated to the etching of amorphous carbon and/or defects on the sidewall which reduce the anchorage site for iron adsorption and secondary growth process.

However, an increase of ethanol concentrations to higher values, i.e. >9 vol.%, leads to a gradual decrease of the VA-MWNTs height (Fig. 2E and G). Similar results have been reported by Zhang et al. [37] and by Pint et al. [38], dealing with the influence of ethanol concentration on the growth rate of VA-CNTs on a planar Fe/Al_2O_3 catalyst. On the other hand, our SEM analyses indicate that at highest ethanol concentration, i.e. 45 vol.%, not only the growth rate but also the CNTs diameter is reduced (Fig. 2H). It is expected that at high ethanol concentration, a large part of the formed CNTs is oxidized by the oxygen generated from the ethanol decomposition which thus, reduces the average height of the CNTs carpet and the diameter of the formed CNTs as well (see Fig. 3B). In the work of Terrones and co-workers [30], for the same concentration of ferrocene, the highest growth rate of the carpet was obtained for the ethanol concentration of only 0.5%, which was far lower compared to the value of 9% observed in this work. In addition, they have reported that the growth process becomes almost nil for ethanol concentration between 2.5 and 8.5 vol.% whereas in this work, the growth process is still operated even at a relatively high ethanol concentration, i.e. 45%. This difference rises probably from a different rate of the injected mixture during the synthesis which influences the contact time between the reactant–SiO_2 support (nanotubes base growth). In order to clarify the additional influence of the H_2 during the synthesis, the same CVD process carried out with 9 vol.% of ethanol without hydrogen was performed. In the absence of H_2, a significant decrease of the growth rate was observed, i.e. 3.8 instead of 18 μm min^{-1} (230/1100 μm of height respectively). The obtained results highlight the synergism effect of hydrogen and ethanol on the growth process of VA-CNTs (Fig. 4C). The SEM

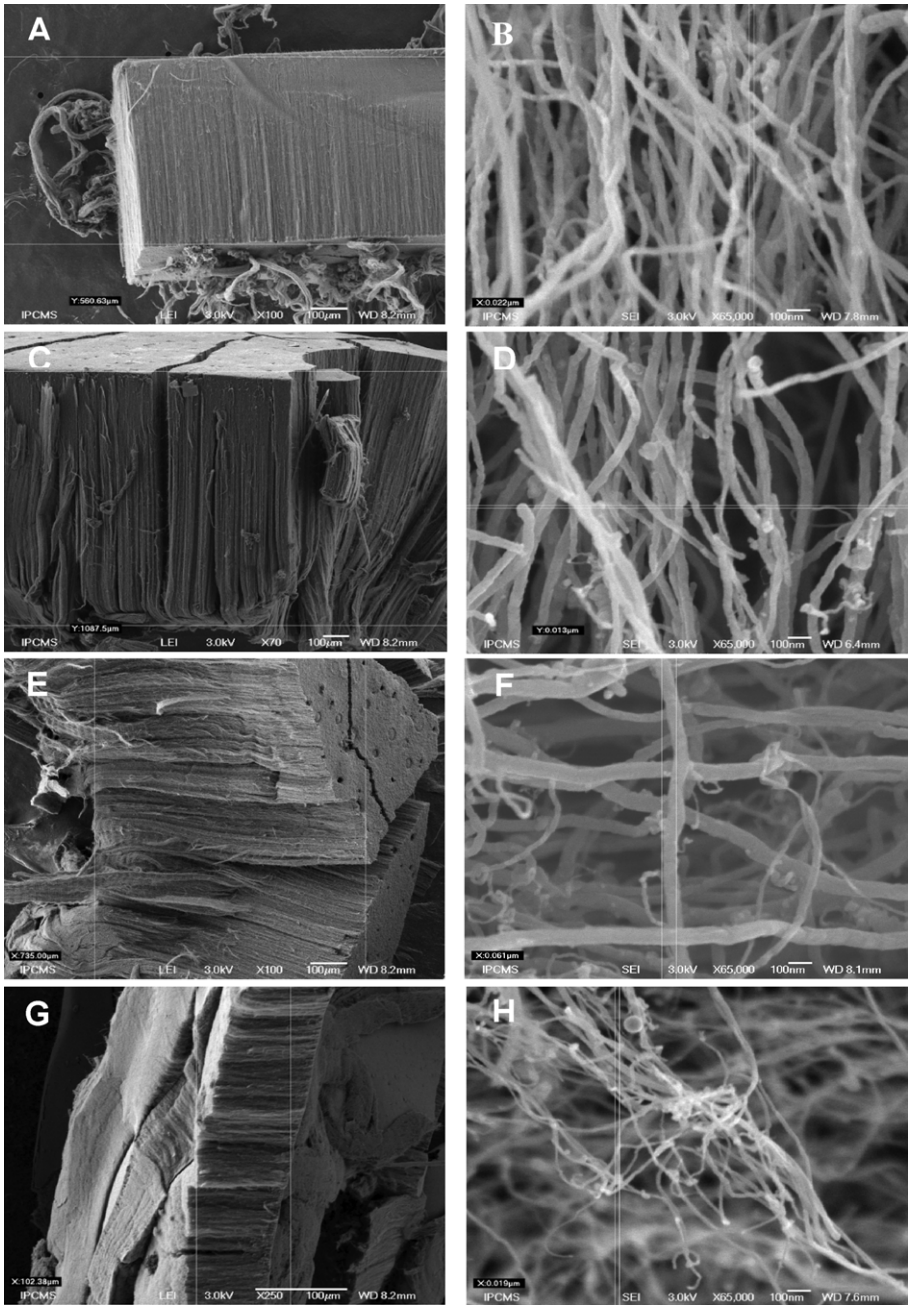

Fig. 2. SEM micrographs of the VA-MWNTs synthesized in the presence of various concentrations of ethanol at 870 °C for 1 h: (a, b) 5 vol.%, (c, d) 9 vol.%, (e, f) 17 vol.%, (g, h) 45 vol.%.

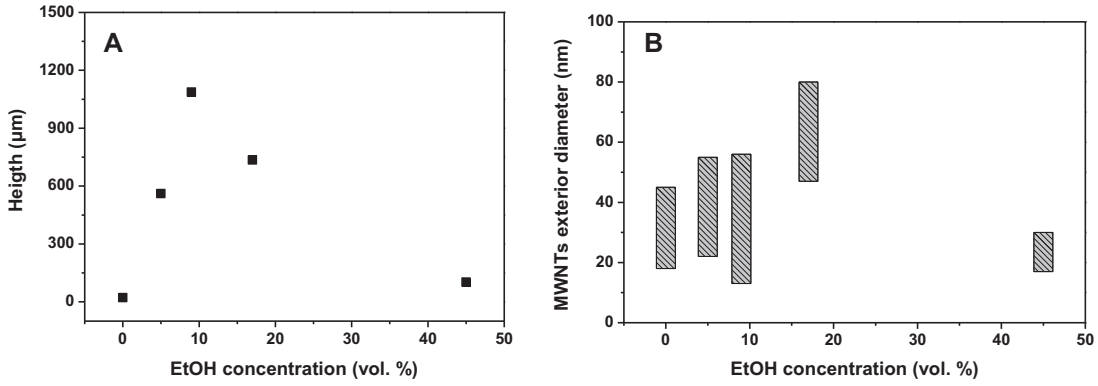

Fig. 3. Influence of ethanol concentration on the average height of VA-MWNTs carpet (A) and on the diameter distribution of nanotubes (B).

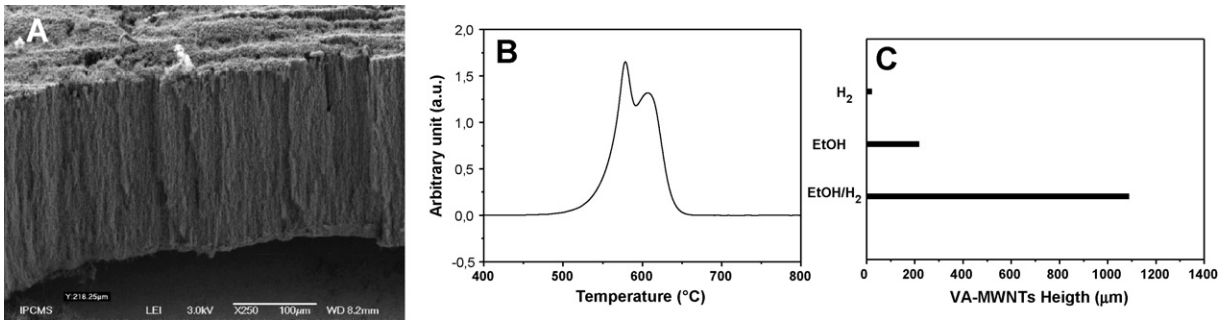

Fig. 4. SEM micrograph and derivation curve from TGA analysis of the nanotubes synthesized with 9% of EtOH without H_2.

micrograph and a derivative of TGA curve of the nanotubes obtained at 0 vol.% of H_2 and 9 vol.% of ethanol are presented in Fig. 4B and C and highlight the presence of a relatively large amount of amorphous carbon in the sample. This demonstrates the effective purifying action of hydrogen to remove amorphous carbon formed during the synthesis.

It is also worthy to note that the carbon nanotubes synthesized at high ethanol concentration exhibit a lower alignment degree than those synthesized at lower ethanol concentration. Such phenomenon could be attributed to the higher degree oxidation of the as-synthesized carbon nanotubes by the oxygenated species generated from the ethanol decomposition.

The specific surface area values of VA-MWNTs are around 54 $m^2\ g^{-1}$ for all synthesis conditions, as shown in Table 1, except the case when 5 vol.% of ethanol is added to the feed. At this ethanol concentration the specific surface area reaches nearly 90 $m^2\ g^{-1}$ which could probably be attributed to the low external diameter of the tubes along with higher volume density of CNTs within the carpet. An apparent density of VA-MWNTs (ρ_v (g/cm^3)) obtained for each ethanol concentration was calculated by dividing the weight of the tubes by the volume of carpet and the results are presented in a Table 1.

The synthesis yield, calculated from the nanotubes weight versus carbon precursor weight (toluene + ethanol) is presented in the same table. The highest yield was obtained with an ethanol concentration centered at around 5 vol.% while the highest aspect ratio was obtained at around 9 ± 5 vol.%. Such results could be attributed to the high density of the CNTs array which is due to the relatively inhibited branching of the as-synthesized carbon nanotubes. It is worthy to note that the presented yields only concern the yields linked with the nanotubes deposited on the silicon substrate regardless the overall mass of the tubes which grown on the inner walls of the quartz reactor. The overall yield of carbon nanotubes deposited after synthesis on the silicon substrate and on the inner wall of the reactor, is much higher (not calculated in this work). The synthesis was carried out with optimized parameters, i.e. synthesis temperature, and reactant mixture flow rate in order to study the influence of the ethanol on the growth rate and morphology of the as-synthesized carbon nanotubes. It is worthy to note that the synthesis parameter concerning the hydrogen concentration was not yet optimized.

Table 1
Influence of the ethanol concentration on the CNTs yield, apparent density and specific surface area.

Ethanol concentration (vol.%)	CNT yield (wt.%)	ρ_v (g/L)	Specific surface area ($m^2\ g^{-1}$)
0	0.002	65	53
5	1.218	1250	83
9	0.174	82	55
17	0.152	94	54

The presence of ethanol and H_2 in the reactant mixture also has a great influence on the oxidation resistance of the synthesized carbon nanotubes according to the DTA results (Fig. 5). The maximum combustion temperature was centered at around 550 °C for the sample synthesized without ethanol and steadily increases to about 650 °C when ethanol was added to the feed with a concentration up to 9 vol.%. At higher ethanol concentration, the oxidation temperature slightly decreased indicating that some structural defects or also additional oxygenated functional groups were formed on the sidewall of the nanotubes. The DTA curves also evidence quite narrow combustion peak for the most graphitized samples, obtained in the presence of 5 and 9 vol.% of ethanol. On the other hand, the enlargement of the DTA peaks for samples synthesized without or with higher ethanol concentration could be due to the formation of tubes with higher amount of oxygenated functional

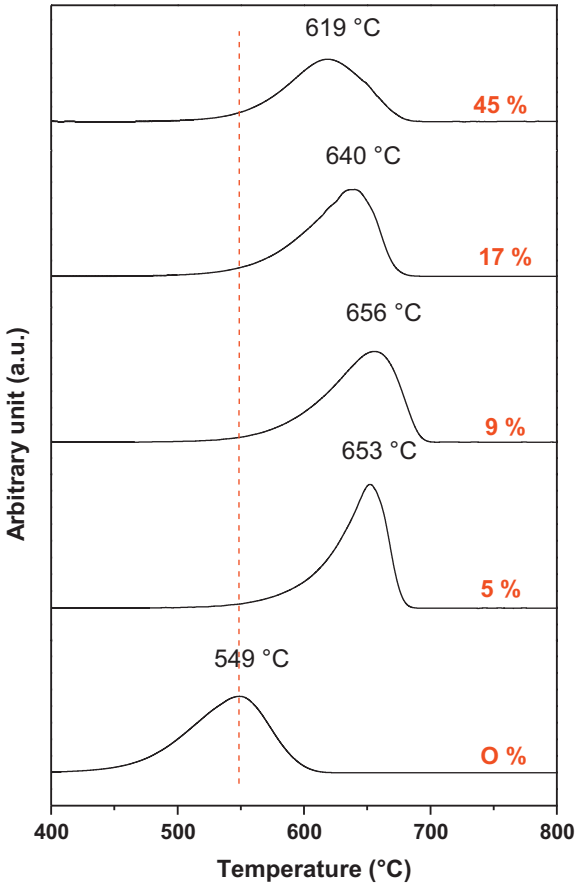

Fig. 5. The TGA (derivation curves) curves of the VA-MWNTs samples as a function of the ethanol concentration in the reactant mixture.

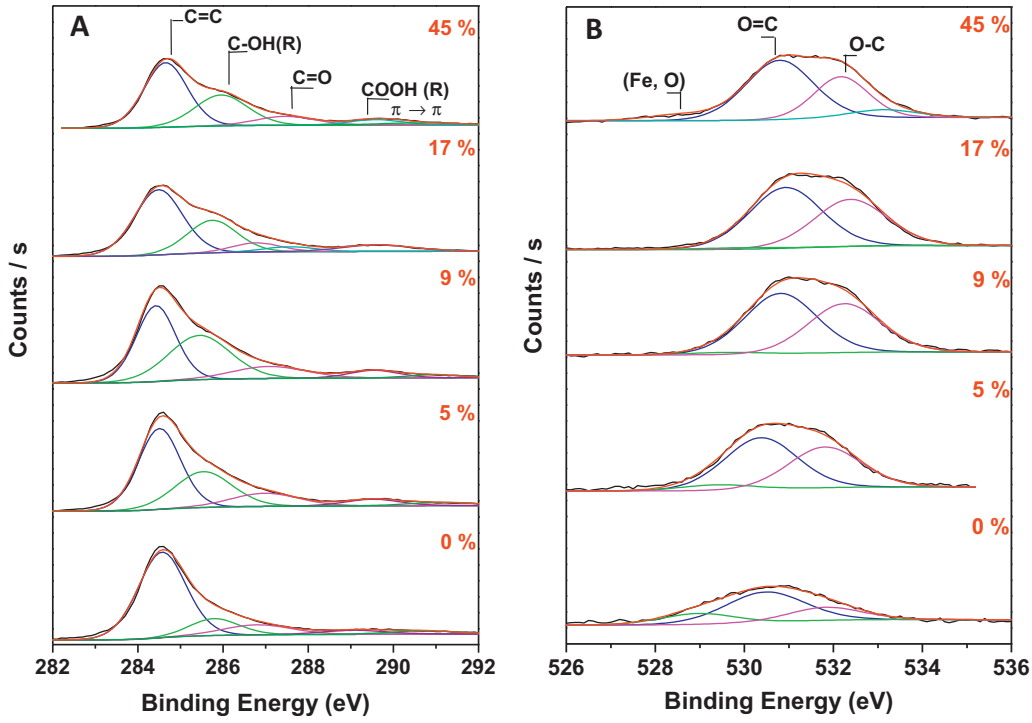

Fig. 6. C1s and O1s XPS spectra of the VA-MWNTs synthesized at different ethanol concentrations.

groups or defects. It should be point out that the percentage of the encapsulated iron in the tubes, remaining from the synthesis and estimated from the DTA analysis (not shown) was the same regardless the ethanol concentration, i.e. 4.0–4.5 wt.%. Such residual iron species were generally localized inside the carbon nanotubes channel and encapsulated by graphene layers and thus remain inaccessible to any gas or liquid for subsequence catalytic applications.

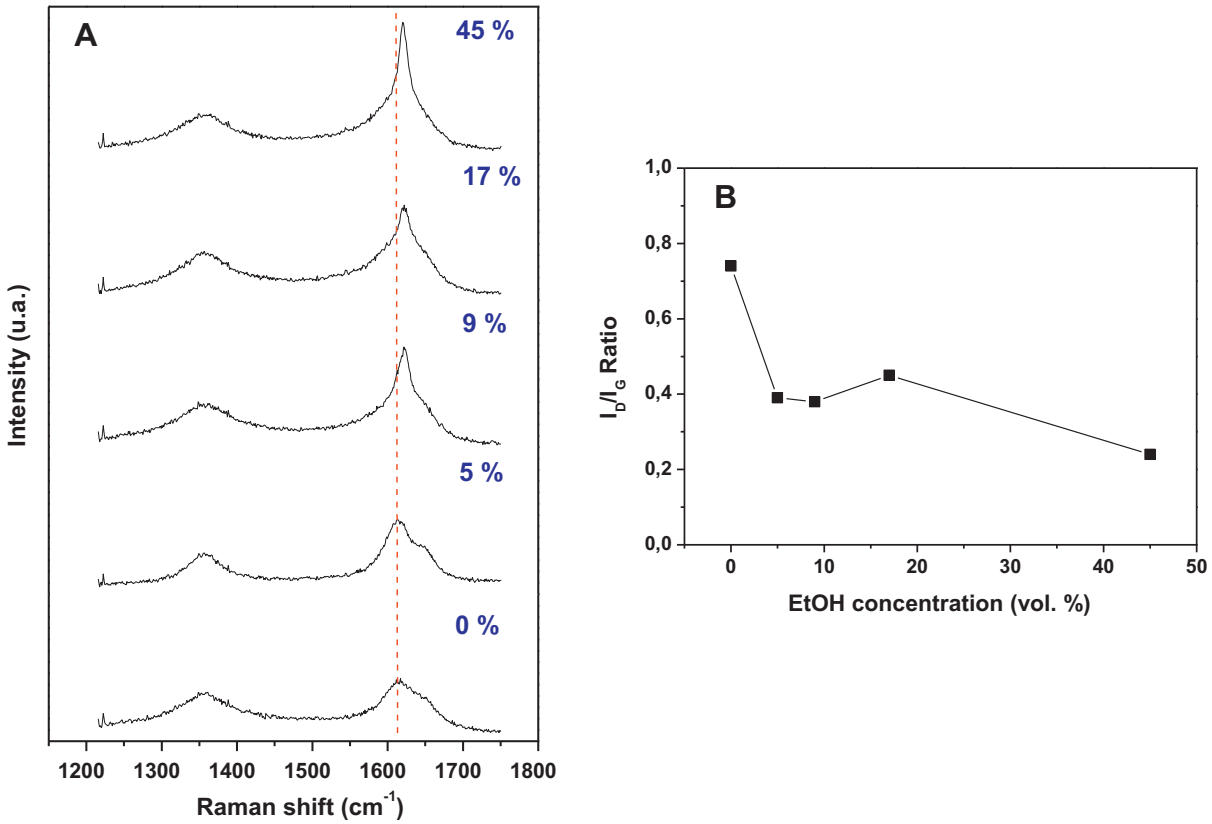

Fig. 7. (a) Raman spectra recorded on the VA-MWNTs samples synthesized with different ethanol concentrations. (b) Evolution of the D/G peak intensity ratio as a function of the ethanol concentrations in the reactant mixture.

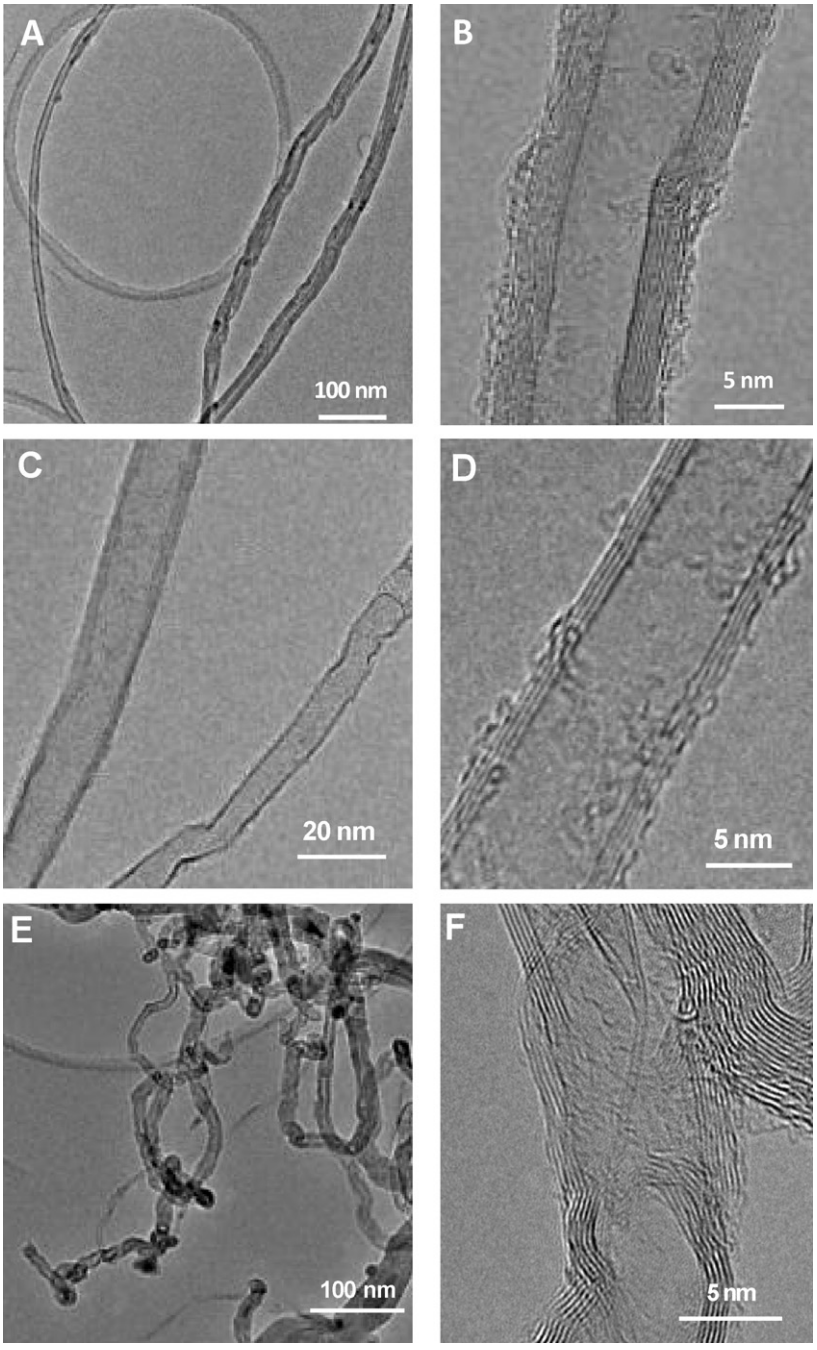

Fig. 8. TEM micrographs of the VA-MWNTs arrays as a function of the ethanol concentration in the processing feed: (A, B) 0%, (C, D) 5%, (E, F) 17%.

The recorded C1s and O1s XPS spectra of the VA-CNTs synthesized at different ethanol concentrations are presented in Fig. 6. The atomic percentage of the various elements, as determined from the spectra areas and relative sensitivity factors, shows the significant and slight increase of C—OH and COOH respectively with increasing ethanol concentration.

The overall O/C atomic also linearly increases with increasing the ethanol concentration in the processing mixture (Table 2). A small amount of iron was also detected by the XPS analysis which could be originated from the residual iron species present within the CNT channel.

Raman spectra recorded on the synthesized samples, presented in Fig. 7A show the increase of the graphitized Raman peak (G peak) [39,40] with the increase of ethanol concentration. Fig. 7B shows the evolution of the I_D/I_G peaks intensity ratio as a function of the ethanol concentration. The I_D/I_G intensity ratio strongly decreases from 0.75 to 0.38 with addition of EtOH to the reactant mixture (5–9 vol.%), which indicates that the as-synthesized carbon nanotubes become more graphitized. Pingheng

Table 2
Carbon and oxygen concentration (at.%) ratio in the VA-MWNTs synthesized with different ethanol content.

Ethanol (vol.%)	C1s (at.%)	O1s (at.%)
0	94	6
5	93	7
9	92	8
17	90	10
45	89	11

et al. [41] reported values of I_D/I_G of 0.051 for highly oriented pyrolytic graphite (HOPG), 0.43 for carbon nanotubes synthesized by D.C. arc discharge and 0.36 for carbon nanotubes synthesized via a CVD method. By comparing the results obtained in the present work with those from Pingheng et al. one can state that the VA-CNTs synthesized in the presence of 9% of ethanol concentration exhibit a relatively high degree of graphitization. The I_D/I_G ratio slightly increases from 0.38 to 0.42 at higher ethanol concentration (17 vol.%), according to the previous study [30], indicating the increased reticular imperfections in the sp^2 network [42,43]. The formation of edge-like defects, vacancies and oxidized sp^3 carbons contribute to this phenomenon. Exceptionally high I_G for the sample with the highest ethanol concentration (45 vol.%) can be related to the highly homogenous chirality of the tubes, as the shape of the peak is very thin, which is not the case for the sample prepared with the low ethanol concentration.

A slight shift of the G band; towards lower values (from 1617 to 1613 cm^{-1}) for the 5% of EtOH, than towards higher values (1622 cm^{-1}) for the 9% and 17% of EtOH and finally towards lower value (1620 cm^{-1}) for the 45% of EtOH also indicates that the disorder degree increase for the important EtOH concentration sample.

TEM micrographs of the samples synthesized with different ethanol concentrations (0, 5 and 17 vol.%) are presented in Fig. 8. TEM analysis indicates that some surface amorphous carbon was observed on the sample synthesized in the absence of ethanol which is in agreement with the DTA (Fig. 8A and B). When ethanol was added to the reactant feed, the TEM examination shows the formation of MWNTs with cleaner surface and among them some tri-walled CNTs with outer and inner diameter of 9 nm and 7 nm, respectively (Fig. 8C and D).

A disordered morphology of the carbon nanotubes obtained in the presence of 17 vol.% of ethanol (Fig. 8E and F) is in agreement with a high concentration of oxygenated groups determined in this sample by the XPS measurements (see Table 2) and a higher degree of oxidation. Indeed, at a relatively high synthesis temperature (870 °C), oxygen species from ethanol could further react with the carbon atoms vacancies, single- or bi-vacancies [44], to form functionalized oxygenated groups or to etch carbon atom leading to the formation of carbon nanotubes with shorter length or sidewall defects.

4. Conclusion

In summary, ethanol can be efficiently employed at low concentration to prevent the active phase encapsulation by amorphous carbon and thus to significantly improve the growth rate of the vertically aligned carbon nanotubes array by a factor of fifty for 9 vol.% of EtOH. Along with an improvement of the specific surface area from 50 to 90 $m^2\,g^{-1}$, the graphitization and oxygenation resistance degree increase with addition of ethanol to the processing mixture. However higher ethanol concentration, >9 vol.%, leads to a gradual decrease of the intrinsic growth rate which is attributed to the excessive oxidation of the formed carbon nanotubes by the oxygen-containing species provided by the decomposition of ethanol. Additional experiments carried out also pointed out the synergism effect between hydrogen and ethanol in the growth process. Indeed, the results have shown that a combination of hydrogen and ethanol allows to growth VA-MWNTs with a high aspect ratio and an improved alignment. Work is on going to get more insight about the role of hydrogen in the reactant mixture.

Acknowledgments

The present work is financially supported by the doctoral scholarship grant of the Algerian Ministry of Higher Education and Scientific Research. The authors would like to acknowledge Dr. F. Antoni (InESS) and M. Th. Romero (LMSPC) for performing Raman and SEM experiments.

References

[1] P. Serp, M. Corrias, P. Kalck, Appl. Catal. A 253 (2003) 337–358.
[2] C. Pham-Huu, M.J. Ledoux, Top. Catal. 40 (2006) 49–63.
[3] P.M. Ayajan, Chem. Rev. 99 (1999) 1787–1800.
[4] J.M. Planeix, N. Coustel, B. Coq, V. Brotons, P.S. Kumbhar, R. Dutartre, P. Geneste, P. Bernier, P.M. Ajayan, J. Am. Chem. Soc. 116 (1994) 7935–7936.
[5] A. Deneuve, I. Florea, O. Ersen, P. Nguyen, C. Pham, D. Begin, D. Edouard, M.J. Ledoux, C. Pham-Huu, Appl. Catal. A 385 (2010) 52–61.
[6] K. Chizari, I. Janowska, M. Houllé, I. Florea, O. Ersen, T. Romero, Appl. Catal. A 380 (2010) 72–80.
[7] H. Tang, J.H. Chen, Z.P. Huang, D.Z. Wang, Z.F. Ren, L.H. Nie, Y.F. Kuang, S.Z. Yao, Carbon 42 (2004) 191–197.
[8] A. Caillard, C. Charles, R. Boswell, P. Brault, C. Coutanceau, Appl. Phys. Lett. 90 (2007) 223119.
[9] J. Jang, D.J. Liu, Carbon 45 (2007) 2843.
[10] M. Maghrebi, A.A. Khodadadi, Y. Mortazavi, M. Rahimi, A. Sane, Z. Tsakadze, S. Mhaisalkar, Mater. Chem. Phys. 124 (2010) 1139–1145.
[11] S.M. Mominuzzaman, I. Khatri, Z. Jianhui, T. Soga, T. Jimbo, ICECE (2008) 287–290.
[12] L. Huang, X. Cui, B. White, S.P.O. Brien, J. Phys. Chem. B 108 (2004) 16451–16456.
[13] W. Zhou, L. Ding, J. Liu, Nano Res. 2 (2009) 593–598.
[14] G. Centi, M. Gangeri, M. Fiorello, S. Perathoner, J. Amadou, D. Begin, M.J. Ledoux, C. Pham-Huu, M.E. Schuster, D.S. Su, J.-P. Tessonnier, R. Schlögl, Catal. Today 147 (2009) 287–299.
[15] A.G. Nasibulin, A. Moisala, H. Jiang, E.I. Kauppinen, J. Nanoparticle Res. 8 (2006) 465–475.
[16] P. Gallezot, D. Richard, Catal. Rev.: Sci. Eng. 40 (1998) 81.
[17] I. Janowska, G. Winé, M.J. Ledoux, C. Pham-Huu, J. Mol. Catal. A: Chem. 267 (2007) 92–97.
[18] H. Chen, A. Roy, J.B. Baek, L. Zhu, J. Qu, L. Dai, Mater. Sci. Eng. 70 (2010) 63–91.
[19] Y.H. Wang, M.J. Kim, H.W. Shan, C. Kittrell, H. Fan, L. Ericson, W.F. Hwang, S. Arepalli, R.H. Hauge, R.E. Smalley, Nano Lett. 5 (2005) 997–1002.
[20] A. Szabo, C. Perri, A. Csato, G. Giordano, D. Vuono, J.B. Nagy, Materials 3 (2010) 3092–3140.
[21] Y.L. Li, L.H. Zhang, X.H. Zhong, A.H. Windle, Nanotechnology 18 (2007) 225604 (6pp).
[22] H. Liu, D. Takagi, H. Ohno, S. Chiashi, T. Chokan, Y. Homma, Appl. Phys. Express 1 (2008) 0140011–0140013.
[23] S. Maruyama, E. Einarsson, Y. Murakami, T. Edamura, Chem. Phys. Lett. 403 (2005) 320–323.
[24] I. Janowska, S. Hajiesmaili, D. Bégin, V. Keller, N. Keller, M.J. Ledoux, C. Pham-Huu, Catal. Today 145 (2009) 76–84.
[25] W. Mi, D. Jia, J. Chil. Chem. Soc. 55 (2010) 153–155.
[26] F. Su, J.N. Wang, F. Yu, Z.M. Sheng, H. Chang, C. Pak, Chem. Phys. Lett. 420 (2006) 421–425.
[27] P.B. Amama, C.L. Pint, L. Mcjilton, S.M. Kim, E.A. Stach, P.T. Murray, R.H. Hauge, B. Maruyama, Nano Lett. 9 (2009) 44–49.
[28] H. Qi, C. Qian, J. Liu, Chem. Mater. 18 (2006) 5691–5695.
[29] S.C. Lyu, T.J. Lee, C.W. Yang, C.J. Lee, Chem. Commun. 12 (2003) 1404–1405.
[30] A.B. Mendez, J.C. Delgado, A.M. Gomez, J.M.R. Herrera, A.G. Rodriguez, H. Navarro, M.A. Vidal, H. Terrones, M. Terrones, Chem. Phys. Lett. 453 (2008) 55–61.
[31] K. Hata, D.N. Futaba, K. Mizuno, T. Namai, M. Yumura, S. Iijima, Science 306 (2004) 1362–1364.
[32] D.N. Futaba, K. Hata, T. Namai, T. Yamada, K. Mizuno, Y. Hayamizu, M. Yumura, S. Iijima, J. Phys. Chem. B 110 (2006) 8035–8038.
[33] G. Ortega-Cervantez, G. Rueda-Morales, J. Ortiz-Lopez, Microelectron. J. 36 (2005) 495–498.
[34] G. Zhang, D. Mann, L. Zhang, A. Javey, Y. Li, E. Yenilmez, Q. Wang, J.P. McVittie, Y. Nishi, J. Gibbons, H. Dai, Proc. Natl. Acad. Sci. U.S.A. 102 (2005) 16141–16145.
[35] H. Sugime, S. Noda, S. Maruyama, Y. Yamaguchi, Carbon 47 (2009) 234–241.
[36] S. Maruyama, R. Kojima, Y. Miyauchi, S. Chiashi, M. Kohno, Chem. Phys. Lett. 360 (2002) 229–234.
[37] Y. Zhang, J.M. Gregoire, R.B. Van Dover, A.J. Hart, J. Phys. Chem. C 114 (2010) 6389–6395.
[38] C.L. Pint, S.T. Pheasant, A.N.G. Parra-Vasquez, C. Horton, Y. Xu, R.H. Hauge, J. Phys. Chem. C 113 (2009) 4125–4133.
[39] M.S. Dresselhaus, G. Dresselhaus, R. Saito, A. Jorio, Phys. Rep. 409 (2005) 47–99.
[40] U.J. Kim, C.A. Furtado, X. Liu, G. Chen, P.C. Eklund, J. Am. Chem. Soc. 127 (2005) 15437–15445.
[41] T. Pingheng, S. Zhang, K.T. Yue, F. Huang, Z. Shi, X. Zhou, J. Raman Spectr. 28 (1997) 369–372.
[42] A.C. Ferrari, J. Robertson, Phys. Rev. B 61 (2000) 14095–14107.
[43] R. Saito, A. Gruneis, G.G. Samsonidze, V.W. Brar, G. Dresselhaus, M.S. Dresselhaus, A. Jorio, L.G. Cancado, C. Fantini, M.A. Pimenta, A.G. Souza Filho, New J. Phys. 5 (2003), pp. 157.1-157.15.
[44] F. Banhart, J. Kotakoski, A.V. Krasheninnikov, ACS Nano 5 (2011) 26–41.